Circrhbdd1 Augments M^{6}a-Dependent Metabolic Reprogramming and Restricts Anti-PD-1 Therapy in Hepatocellular Carcinoma

Juan Cai

The First Affiliated Hospital of Wannan Medical College: Yijishan Hospital of Wannan Medical College
https://orcid.org/0000-0001-7996-2525

Zhiqiang Chen

Jiangsu Province Hospital and Nanjing Medical University First Affiliated Hospital

Yao Zhang

Jiangsu Province Hospital and Nanjing Medical University First Affiliated Hospital

Jinguo Wang

The First Affiliated Hospital of Wannan Medical College: Yijishan Hospital of Wannan Medical College

Junfeng Wang

The First Affiliated Hospital of Wannan Medical College: Yijishan Hospital of Wannan Medical College

Zhengrong Zhang

The First Affiliated Hospital of Wannan Medical College: Yijishan Hospital of Wannan Medical College

Haoran Li

The First Affiliated Hospital of Wannan Medical College: Yijishan Hospital of Wannan Medical College

Jindao Wu

Jiangsu Province Hospital and Nanjing Medical University First Affiliated Hospital

Jiading Mao

The First Affiliated Hospital of Wannan Medical College: Yijishan Hospital of Wannan Medical College

Xuehao Wang

Jiangsu Province Hospital and Nanjing Medical University First Affiliated Hospital

Xueliang Zuo (✉ zuoxueliang0202@126.com)

Jiangsu Province Hospital and Nanjing Medical University First Affiliated Hospital
https://orcid.org/0000-0001-5204-2585

Research

Abstract

Background

Metabolic rewiring of cancer cells reshapes the tumor microenvironment, thereby restricting the response to immunotherapy. Circular RNAs (circRNAs) can influence various cellular processes and have been implicated in hepatocellular carcinoma (HCC). Here, we investigated the role of a novel circRNA circRHBDD1 in HCC metabolic transformation and immunotherapy resistance.

Methods

CircRNA sequencing was performed to determine the differentially expressed circRNA profile in HCC. RT-qPCR and *in situ* hybridization were used to verify the dysregulation of circRHBDD1 in two independent HCC cohorts. Univariate and multivariate survival analyses were employed to assess the prognostic significance of circRHBDD1. Loss- and gain-of-function approaches were adopted to evaluate the effects of circRHBDD1 on glycolysis and glutaminolysis. Patient-derived xenograft models were used for *in vivo* evaluation. RNA pull-down, mass spectrometry, RNA immunoprecipitation, fluorescence *in situ* hybridization, polysome profiling, and meRIP assays were utilized to explore the molecular mechanisms of circRHBDD1 in HCC.

Results

We found that circRHBDD1 was significantly upregulated in HCC and associated with unfavorable clinicopathological characteristics and poor survival outcomes. *In vitro* and *in vivo* experiments showed that circRHBDD1 facilitated HCC glycolysis and glutaminolysis. Mechanistic studies revealed that circRHBDD1 could recruit YTHDF1 to PIK3R1 mRNA and augment PIK3R1 translation in an m^6A-dependent manner, leading to activation of the PI3K/AKT signaling. EIF4A3-mediated exon back-splicing contributed to the upregulation of circRHBDD1. Moreover, targeting of circRHBDD1 was able to improve anti-PD-1 therapy resulting in prolonged survival.

Conclusion

We identified that the circRHBDD1/YTHDF1/PIK3R1 axis was crucial to metabolic reprogramming of HCC. Suppression of circRHBDD1 could potentially sensitize HCC cells to anti-PD-1 therapy.

Background

Hepatocellular carcinoma (HCC) ranks sixth in terms of incidence and is the third leading cause of cancer-related death worldwide [1]. Most patients with HCC are diagnosed at an advanced stage. Despite the progresses made in HCC treatment, the 5-year survival rate remains dismal. Hence, elucidating its

underlying mechanisms and identifying novel prognostic biomarkers and therapeutic candidates exhibit paramount significance.

Behind the malignant phenotypes of HCC lie multiple genetic mutations contributing to the reprogramming of cancer cell metabolism. Recognized as a major hallmark of cancer, cellular metabolic alternations impinge on multiple core pathways such as glucose and amino acid metabolism [2]. Instead of complete oxidation through the tricarboxylic acid cycle, cancer cells tend to convert glucose to lactate through accelerated aerobic glycolysis. While enhanced glycolysis satisfies the increasing demands for energy of cancer cells, augmented glutamine metabolism supplies cancer cells with biosynthetic precursors. Glutamine has been considered a crucial amino acid that provides carbon and nitrogen to cancer cells to sustain anabolic biosynthesis. Tumor cells shift to increased rates of glutaminolysis through accelerated conversion of glutamine to glutamate and subsequent production of α-ketoglutarate (α-KG) for the tricarboxylic acid cycle. Inhibition of glycolysis and glutaminolysis has provided an emerging field of novel drug discovery [3].

Circular RNAs (circRNAs) are a class of covalent closed RNA transcripts generated from the back-splicing of pre-mRNA. CircRNAs are abundant, stable, evolutionarily conserved, and present spatiotemporally-specific expression patterns [4]. As indispensable regulators in various physiological and pathological processes, circRNAs function through diverse mechanisms, including acting as microRNA sponges, interacting with RNA-binding proteins, regulating gene transcription, and translating into peptides. Accumulating evidence has cast light on the involvement of circRNAs in metabolic reprogramming of cancer cells. In neuroblastoma, circ-CUX1 facilitates aerobic glycolysis through binding to EWSR1 [5]. Our previous study indicated that circHECTD1 promoted glutaminolysis by targeting USP5 in gastric cancer [6]. It is worthwhile to investigate the effects of circRNAs in these altered metabolic processes underlying HCC progression.

Here, we demonstrated that the upregulation of circRHBDD1 orchestrated glycolysis and glutaminolysis in HCC and independently predicted patient survival outcomes. *In vivo* experiments with patient-derived xenograft (PDX) mouse models confirmed the tumor-promoting effects of circRHBDD1. Mechanistically, circRHBDD1 directly interacted with YTHDF1, promoted the N^6-methyladenosine (m^6A) modification of PIK3R1 mRNA, and accelerated PIK3R1 translation to allow for activation of the PI3K/AKT signaling pathway. EIF4A3 induced the upregulation of circRHBDD1 in HCC. Moreover, we found that targeting of circRHBDD1 could enhance the response to anti-PD-1 therapy. This study may provide a better insight into the roles of circRNAs in HCC metabolic reprogramming and immunotherapy.

Methods

Patients and tissue samples

To determine circRHBDD1 expression, two independent cohorts of HCC patients were enrolled in this study. For the first cohort (cohort 1), 96 paired HCC tissues and corresponding adjacent tissues were

collected from patients who received hepatectomy at the First Affiliated Hospital of Nanjing Medical University from 2017 to 2019. The second cohort (cohort 2) used for tissue microarray (TMA) analysis consisted of 160 HCC patients undergoing hepatectomy between 2010 and 2015 at the First Affiliated Hospital of Wannan Medical College. Patients enrolled in cohort 2 were followed up for survival analysis. All included patients had not received chemotherapy or radiotherapy before surgery. Written informed consents were obtained from all patients before enrollment. The study protocol was approved by the Ethics Committee of the First Affiliated Hospital of Nanjing Medical University and the Ethics Committee of the First Affiliated Hospital of Wannan Medical College. This study was conducted in accordance with the Declaration of Helsinki.

CircRNA sequencing

CircRNA sequencing using three paired HCC tissues and adjacent liver tissues was performed by RiboBio (Guangzhou, China). Briefly, total RNA was extracted from HCC tissues and adjacent tissues using TRIzol reagent (Invitrogen, Carlsbad, CA, USA). RNA purity was assessed using ND-1000 Nanodrop, and an Agilent 2200 TapeStation (Agilent Technologies, Santa Clara, CA, USA) was adopted to detect RNA integrity. An Epicentre Ribo-Zero rRNA Removal Kit (Illumina, San Diego, CA, USA) was employed for rRNA removal. RNase R (Epicentre Technologies, WI, USA) was used to degrade linear RNA. According to the protocols of the NEBNext® Ultra™ RNA Library Prep Kit for Illumina, adaptor ligation and enrichment with a low cycle were performed. Then, the purified RNA was used for cDNA synthesis and sequencing. CIRI2 and CIRCexplorer2 algorithms were adopted to determine circRNAs. Differentially expressed circRNAs ($P <$ 0.05 and fold change > 2) were identified based on the DESeq2 package.

RNA extraction, RNase R treatment, and quantitative real-time polymerase chain reaction (RT-qPCR)

Total RNA was extracted from tissues and cells using TRIzol reagent (Invitrogen). For RNase R treatment, 2 µg of total RNA was incubated with 3 U/µg of RNase R (Epicentre Technologies) for 15 min at 37°C. Reverse transcription was conducted using the PrimeScript RT Master Mix (TaKaRa, Dalian, China). qPCR was performed using TB Green Premix Ex Taq (TaKaRa) on ABI 7900HT (Applied Biosystems, Foster City, CA, USA). The primers for RT-qPCR used in this study are listed in Additional file 1: Table S1.

Fluorescence *in situ* hybridization (FISH) and immunofluorescence

Cells and tissues were fixed with 4% paraformaldehyde, permeabilized with 0.5% Triton X-100 in phosphate-buffer saline, and then incubated in hybridization buffer with circRHBDD1 probes overnight. DAPI was used to stain the nuclei. All images were analyzed on a fluorescence microscope (Leica Microsystems, Mannheim, Germany). Specific FISH probe to circRHBDD1 was designed and synthesized by RiboBio.

For immunofluorescence assay, cells were fixed in a 4% paraformaldehyde solution, permeabilized in phosphate-buffer saline with 0.5% Triton X-100, blocked in 3% bovine serum albumin, and then incubated

with the primary antibody against YTHDF1 at 4°C overnight. Followed by incubation with the secondary antibody, the cells were photographed under a fluorescence microscope (Leica Microsystems).

RNA *in situ* hybridization (ISH)

HCC samples and the corresponding adjacent liver tissues in cohort 2 were used for TMA construction. After blocking endogenous peroxidase by 3% methanol-H_2O_2, the TMAs were hybridized with digoxin-labelled circRHBDD1 probe (RiboBio) at 37°C overnight. TMAs were incubated in bovine serum albumin for 30 min and anti-digoxin labelled peroxidase at 37°C for 40 min, and then stained with diaminobenzidine solution. Images were obtained under microscope (Nikon Corporation, Japan), and ISH intensity scores were defined as follows: 0 (weak), 1 (moderate), 2 (strong), and 3 (very strong).

Seahorse metabolic analysis

The extracellular acidification rate (ECAR) and cellular oxygen consumption rate (OCR) were measured using Seahorse XF Glycolysis Stress Test Kit and Seahorse XF Cell Mito Stress Test Kit (Agilent Technologies) according to the manufacturer's protocols. In brief, 1×10^4 cells/well were seeded into Seahorse XF 96-cell culture plates and then loaded into the Seahorse XF 96 Extracellular Flux Analyzer (Agilent Technologies). For ECAR measurement, glucose, the oxidative phosphorylation inhibitor oligomycin, and the glycolytic inhibitor 2-deoxyglucose (2-DG) were sequentially added at indicated time points. Oligomycin, the mitochondrial uncoupler carbonyl cyanide p-trifluoromethoxy phenylhydrazone (FCCP), and the mitochondrial complex III inhibitor antimycin A plus the mitochondrial complex I inhibitor rotenone were sequentially injected for OCR detection.

Measurement of lactate production, cellular glucose-6-phosphate (G6P), and ATP levels

Cells were seeded into 96-well cell culture plates and incubated overnight. After starvation for 2 h, the supernatant was harvested for measurement of lactate production using the L-Lactate Assay Kit (Abcam, Cambridge, UK). The levels of cellular G6P were measured using a Glucose-6-phosphate Fluorometric Assay Kit (Cayman, Ann Arbor, MI, USA), and ATP determination Kit (Thermo Fisher Scientific, CA, USA) were used to determine ATP levels according to the manufacturer's instructions.

Analyses of glutamine, glutamate, and α-KG levels

Cells were plated into 6-well plates and cultured for 24 h. Concentrations of glutamine and glutamate were measured by a Glutamine/Glutamate Determination Kit (Sigma-Aldrich, St. Louis, MO, USA) in accordance with the manufacturer's protocol. We used α-KG Assay Kit (Abcam) to detect the α-KG level based on the manufacturer's protocols.

RNA immunoprecipitation (RIP) and methylated RNA immunoprecipitation (meRIP) assays

RIP assays were performed using a Magna RIP RNA-Binding Protein Immunoprecipitation Kit (EMD Millipore, Billarica, MA, USA) according to the manufacturer's instructions. Briefly, cells were lysed using

RIP lysis buffer containing protease and RNase inhibitors (EMD Millipore). Then, the cell lysates were incubated with antibodies against AGO2 (ab186733, Abcam), EIF4A3 (ab32485, Abcam), Flag (F1804, Sigma-Aldrich), or nonspecific IgG antibody (#12-371, EMD Millipore) at 4°C overnight, respectively. MeRIP assay was conducted using a Magna MeRIP m^{6}A Kit (EMD Millipore) based on the manufacturer's protocol. The immunoprecipitated RNA was isolated and subjected to RT-qPCR analysis.

RNA pull-down assay

CircRHBDD1 pull-down assay was performed using a Magnetic RNA-protein Pull-down Kit (Thermo Fisher Scientific) in accordance with the manufacturer's protocol. The biotin-labelled sense and antisense probes were designed and synthesized by RiboBio. Briefly, total RNA was incubated with biotin-labelled probes for 5 min and Streptavidin Magnetic Beads (Invitrogen) for 30 min with rotation. Unbound RNA was washed away and RNA-protein binding buffer was added. Supernatant was obtained for silver staining, mass spectrometry, and western blotting.

PDX mouse model

We used NOD/SCID and BALB/c mice to construct the PDX models of HCC as previously described [7]. Briefly, primary tumor tissues from HCC patients undergoing hepatectomy were kept in iced culture medium supplemented with 1% penicillin/streptomycin, and cut into approximately 2-3 mm^3 fragments in 100 µl 50% Matrigel (BD Biosciences, San Jose, CA, USA). Then the tissue samples were implanted subcutaneously into the flanks of NOD/SCID mice. Engrafted tumors were harvested when they grew up to 1-2 cm^3, and spliced up for the serial transplantation in BALB/c nude mice. When the engrafted tumor volume reached around 50 mm^3, intratumoral injection of the circRHBDD1 plasmid, cholesterol-conjugated circRHBDD1 siRNA or the corresponding controls was performed continuously for 3 weeks. Tumor volume and weight were measured, and the tumors were processed for RT-qPCR, FISH, and immunohistochemistry (IHC) assays.

Statistical analysis

Statistical analyses were performed using SPSS 26.0 (IBM Corporation, Armonk, NY, USA) and GraphPad Prism 8.0 (GraphPad Software, La Jolla, CA, USA) software. Data are shown as mean ± standard error of mean. Two-sided Student's *t* test was used to analyze the differences between groups. Paired *t* test was used to evaluate the differences of circRNA expression levels between tumor and peritumor samples. Chi-square test or Fisher's exact test was adopted to analyze the association of circRHBDD1 level with clinicopathological variables. Survival distributions were estimated by Kaplan-Meier curve with log-rank test. The prognostic value of circRHBDD1 was assessed using Cox proportional hazards model. The correlation between EIF4A3 and circRHBDD1 levels was analyzed using Pearson's correlation coefficient. A two-tailed $P < 0.05$ was considered statistically significant. * $P < 0.05$; ** $P < 0.01$; *** $P < 0.001$; ns, no significance.

Additional experimental details are included in Additional file 2: Supplementary methods.

Results

CircRHBDD1 is highly expressed in HCC and predicts unfavorable patient survival

We compared the circRNA expression profiles between three paired HCC tissues and adjacent liver tissues using circRNA sequencing analysis. A total of 7,747 distinct circRNA candidates with ≥ 2 unique back-splicing junction reads were detected by both CIRI2 and CIRCexplorer2 algorithms. Of these, 5,010 were annotated in circBase. The DESeq2 package was further applied to identify the differentially expressed circRNAs. As illustrated in Fig. 1a and b, 44 and 65 circRNAs were upregulated and downregulated in HCC tissues, respectively. Among them, the top five upregulated circRNAs were validated by RT-qPCR in 20 matched HCC and peritumor tissues which were randomly chosen from cohort 1 (Fig. 1c). We found that hsa_circ_0058497, which derived from *RHBDD1* gene locus and was hereafter referred to as circRHBDD1, exhibited the most prominent upregulation, and was selected for further study. In consistence with the results from HCC tissue samples, the expression level of circRHBDD1 was significantly higher in a panel of human HCC cell lines compared to the normal human liver cell line (Fig. 1d).

Divergent PCR followed by Sanger sequencing analysis revealed that circRHBDD1 was generated from the exon 6-8 of *RHBDD1* gene through back-splicing mechanism (Fig. 1e). Agarose gel electrophoresis assays showed that divergent primers could amplify circRHBDD1 in cDNA, but no product was detected in gDNA (Fig. 1f and g). RT-qPCR using oligo dT primers indicated that circRHBDD1 possessed no poly(A) tail (Fig. 1h). As shown in Fig. 1i, circRHBDD1 resisted RNase R-mediated digestion, whereas the linear form of RHBDD1 products could not endure RNase R treatment. The stability of circRHBDD1 was examined by transcription inhibitor actinomycin D treatment. Our results indicated that the circular isoform was more stable than the linear counterpart (Fig. 1j and k). RNA FISH suggested the predominant cytoplasmic distribution of circRHBDD1 in HCCLM3 cells (Fig. 1l). The fractionation experiment demonstrated that circRHBDD1 was mainly located in the cytoplasm rather than the nucleus (Fig. 1m and n).

To further investigate the clinical value of circRHBDD1 in HCC, we examined the expression of circRHBDD1 in cohort 1 consisting of 96 paired HCC tissues and peritumor specimens. RT-qPCR confirmed that circRHBDD1 was highly expressed in HCC tissues compared with peritumor samples (Fig. 2a). The overexpression of circRHBDD1 in HCC tissues was further verified using FISH analysis (Fig. 2b). The patients from cohort 1 were divided into high and low circRHBDD1 expression groups according to the median expression value. As shown in Additional file 3: Table S2, circRHBDD1 expression level was associated with tumor number ($P = 0.013$), microvascular invasion ($P = 0.002$), tumor size ($P = 0.007$), α-fetoprotein ($P = 0.014$), and tumor-node-metastasis (TNM) stage ($P = 0.001$). Marked upregulation of circRHBDD1 was witnessed in HCC patients with tumor size > 5 cm and those at TNM III-IV stage (Fig. 2c and d). An independent cohort 2 comprised 160 matched HCC and peritumor samples with complete follow-up data was used for TMA analysis. A scoring system based on ISH staining intensity was employed, and the expression level of circRHBDD1 was higher in tumor samples compared to peritumor specimens (Fig. 2e). To determine the prognostic role of circRHBDD1 in HCC patient survival, univariate

and multivariate survival analyses were performed. Kaplan-Meier survival plots showed that high circRHBDD1 expression level was correlated to poor overall survival and disease-free survival (Fig. 2f and h). As shown in Fig. 2g and i and Additional file 4: Table S3, Cox proportional hazards regression analyses indicated that circRHBDD1 expression level was an independent prognostic factor for overall survival [Hazard ratio (HR): 1.549, 95% confidence interval (CI): 1.046-2.293; P = 0.029] and disease-free survival (HR: 2.388, 95% CI: 1.417-4.024; P = 0.001). Taken together, these results suggested that circRHBDD1 was upregulated in HCC tissues and cell lines, and high circRHBDD1 expression predicted unfavorable patient survival outcomes.

CircRHBDD1 promotes glycolysis and glutaminolysis in HCC

To explore the functions of circRHBDD1 in HCC, we sought to characterize the altered cellular phenotypes in HCC cells with circRHBDD1 knockdown or overexpression. We designed two lentiviruses targeting the back-spliced sequence of circRHBDD1. The knockdown efficiency was tested by RT-qPCR in two HCC cell lines (HCCLM3 and MHCC97H). As shown in Fig. 3a and b, sh-circRHBDD1#1 and sh-circRHBDD1#2 remarkably inhibited the expression of circRHBDD1 but not that of RHBDD1 mRNA. Significant reduction on the cell proliferation in HCCLM3 and MHCC97H cells after circRHBDD1 knockdown was detected by colony formation assay (Fig. 3c). Cell Counting Kit-8 (CCK-8) assay showed that silencing circRHBDD1 remarkably suppressed HCC cell viability (Fig. 3d and e). 5-ethynyl-2'-deoxyuridine (EdU) imaging analysis confirmed the inhibitory effects of circRHBDD1 knockdown on HCC cells (Fig. 3f). We further overexpressed circRHBDD1 in HepG2 and Huh7 cells using lentiviruses. As indicated in Additional file 5: Fig. S1A and B, the specific overexpression of circRHBDD1 in HepG2 and Huh7 cells was verified, whereas the expression levels of linear RHBDD1 were consistently unaffected. In consistence with the knockdown experiments, circRHBDD1 upregulation significantly enhanced the proliferative capability of HCC cells by colony formation, CCK-8, and EdU assays (Additional file 5: Fig. S1C-F). These findings indicated that circRHBDD1 promoted HCC viability *in vitro*.

Next, we performed RNA-seq analysis on circRHBDD1-silenced HCCLM3 cells and the corresponding control cells (Fig. 4a). KEGG analysis showed that PI3K-AKT signaling pathway, metabolic pathways, glycolysis/gluconeogenesis, D-glutamine and D-glutamate metabolism were among the enriched pathways (Fig. 4b), indicating a potential role of circRHBDD1 in glucose and glutamine metabolic reprogramming. Then, we detected the mRNA levels of several key transporters and enzymes in glycolysis and glutaminolysis, including GLUT1, HK2, ASCT2, and GLS1, in circRHBDD1-silenced HCCLM3 and MHCC97H cells. CircRHBDD1 knockdown was associated with decreased mRNA levels of GLUT1, HK2, ASCT2, and GLS1 (Fig. 4c and d, Additional file 6: Fig. S2A and B). Moreover, western blotting assays showed that the protein levels of these transporters and enzymes were reduced in HCCLM3 and MHCC97H cells with circRHBDD1 knockdown (Fig. 4e and Additional file 6: Fig. S2C). As indicated by the ECAR data, knockdown of circRHBDD1 significantly reduced glycolysis rate and glycolytic capacity of HCCLM3 and MHCC97H cells (Fig. 4f and Additional file 6: Fig. S2D). As an indicator of mitochondrial respiration, OCR was increased in circRHBDD1-silenced HCCLM3 and MHCC97H cells (Fig. 4g and Additional file 6: Fig. S2E). In 22 HCC patients who received preoperative ^{18}F-FDG PET/CT imaging, we

found that the SUVmax was considerably higher in patients from the cicRHBDD1^{high} group than in those from the circRHBDD1^{low} group (Fig. 4h and i). The levels of glycolysis and glutaminolysis metabolites were analyzed, and the results showed that circRHBDD1 knockdown led to decreased levels of G6P, lactate, ATP, glutamine, glutamate, and α-KG (Fig. 4j and k, Additional file 6: Fig. S2F and G).

Consistently, circRHBDD1 overexpression in HepG2 and Huh7 cells resulted in increased mRNA and protein levels of transporters and enzymes in glycolysis and glutaminolysis (Additional file 7: Fig. S3A-C). Elevated EACR was observed in circRHBDD1-overexpressed HCC cells (Additional file 7: Fig. S3D). Based on the OCR results, basal respiration and maximum respiratory were decreased after circRHBDD1 upregulation (Additional file 7: Fig. S3E). As indicated in Additional file 7: Fig. S3F and G, circRHBDD1 overexpression significantly promoted the levels of glycolysis and glutaminolysis metabolites.

CircRHBDD1 facilitates HCC tumor growth *in vivo*

PDX mouse models were utilized to investigate the effects of circRHBDD1 on HCC growth using 10 fresh HCC tissues from patients undergoing hepatectomy (Fig. 5a). CircRHBDD1 expression levels were detected in the engrafted tumors using RT-qPCR. As indicated in Fig. 5b, xenografts derived from patient #5 had the highest expression level of circRHBDD1, while the engrafted tumors originating from patient #2 exhibited the lowest circRHBDD1 level. The engrafted tumors from patient #5 and #2 were histopathologically analyzed (Fig. 5c). We injected the circRHBDD1 plasmid and cholesterol-conjugated circRHBDD1 siRNA into tumor tissues continuously for 3 weeks. The xenograft tumor volume and weight were markedly reduced in the si-circRHBDD1-treated groups (Fig. 5d-f). Conversely, the xenografts injected with circRHBDD1 plasmid were larger and heavier (Fig. 5d-f). RT-qPCR and FISH assays were used to confirm the consistent knockdown or overexpression of circRHBDD1 in engrafted HCC tumors (Fig. 5g and h). As indicated in Fig. 5i, we found decreased expression levels of GLUT1, ASCT2, and Ki-67 in circRHBDD1-silenced xenografts, whereas elevated GLUT1, ASCT2, and Ki-67 levels were observed in xenografts treated with circRHBDD1 plasmid based on the IHC results.

CircRHBDD1 activates the PI3K/AKT signaling via augmenting PIK3R1 translation

As demonstrated in Fig. 4b, the PI3K/AKT signaling pathway was among the top canonical pathways upon circRHBDD1 knockdown. Next, we performed western blotting analysis to verify that circRHBDD1 knockdown inhibited the PI3K/AKT signaling (Fig. 6a). Previous studies by our lab and others revealed that PIK3R1, a regulatory subunit of PI3K, is an important upstream molecule of the PI3K/AKT signaling during HCC progression [8, 9]. We wondered whether PIK3R1 could be affected by circRHBDD1. As shown in Fig. 6b, PIK3R1 protein levels were decreased after circRHBDD1 was silenced in HCCLM3 and MHCC97H cells. IHC analysis of PDX confirmed that circRHBDD1 knockdown was associated with decreased PIK3R1 and p-AKT levels, while PIK3R1 and p-AKT levels were elevated in circRHBDD1-overexpressing xenografted tumors (Fig. 6c). Intriguingly, PIK3R1 mRNA levels were not altered in circRHBDD1-silenced cells compared with controls (Fig. 6d). There was no apparent difference in the degradation of PIK3R1 protein after circRHBDD1 knockdown (Fig. 6e and f). Moreover, proteasome

inhibitor MG132 and autophagy inhibitor chloroquine (CQ) could not reverse the downregulation of PIK3R1 protein induced by circRHBDD1 knockdown (Fig. 6g). Based on these results, we hypothesized that circRHBDD1 augmented PIK3R1 protein expression possibly via translational control. Therefore, we collected mono/polysome fractions from cytoplasmic extracts of sh-circRHBDD1#1 and sh-NC HCCLM3 cells by sucrose gradient centrifugation. As shown in Fig. 6h, circRHBDD1 knockdown significantly suppressed the proportion of PIK3R1 mRNA in the polysome fraction, whereas the presence of PIK3R1 mRNA in non-translating ribosome fractions was increased.

We then performed rescue experiments by overexpressing PIK3R1 in circRHBDD1-silenced HCCLM3 cells. The overexpression efficiency was confirmed by western blotting (Additional file 8: Fig. S4A). CCK-8 and EdU assays demonstrated that PIK3R1 upregulation rescued the inhibited cell proliferation in sh-circRHBDD1#1 HCCLM3 cells (Additional file 8: Fig. S4B and C). According to the ECAR and OCR data, glycolysis rate, glycolystic capacity, basal respiration, and maximum respiratory were restored after PIK3R1 overexpression in circRHBDD1-silenced HCCLM3 cells (Additional file 9: Fig. S5A and B). In circRHBDD1-silenced cells, upregulation of PIK3R1 abolished the reduction of the levels of glycolysis and glutaminolysis metabolites (Additional file 9: Fig. S5C and D). As indicated in Additional file 9: Fig. S5E, expression levels of the key transporters and enzymes in glycolysis and glutaminolysis, as well as p-AKT levels, were restored after PIK3R1 upregulation in circRHBDD1-silenced cells. Taken together, circRHBDD1 augmented PIK3R1 mRNA translation and was associated with the activation of the PI3K/AKT signaling in HCC.

CircRHBDD1 interacts with YTHDF1 and promotes the translation of PIK3R1 in an m^{6}A-dependent manner

To delineate how circRHBDD1 facilitated the translation of PIK3R1 mRNA, we performed AGO2-RIP assay and the results suggested that circRHBDD1 might not function as a microRNA sponge (Fig. 6i). CPAT bioinformatics prediction results indicated that circRHBDD1 could not encode peptides (Fig. 6j). Then, we conducted RNA pull-down assay combined with mass spectrometry. As shown in Fig. 6k and l, YTHDF1 was identified to interact with circRHBDD1. RIP assay further confirmed the interaction between YTHDF1 and circRHBDD1 (Fig. 6m). Results from FISH assay showed that circRHBDD1 co-localized with YTHDF1 in HCCLM3 cells (Fig. 6n). Bioinformatics analysis indicated that YTHDF1 was upregulated in HCC tissues compared with the peritumor tissues (Fig. 6o), and associated with unfavorable overall survival in HCC patients (Fig. 6p), which were consistent with previous studies [10, 11].

Given that YTHDF1 has been well established as an m^{6}A-binding protein which facilitates translation of m^{6}A-modified mRNA [12, 13], we postulated that YTHDF1 could enhance PIK3R1 translation via m^{6}A modification. Results from the REPIC database [14] suggested the presence of two m^{6}A peaks in PIK3R1 (chr5: 68226662-68226933, chr5: 68298071-68298312). RMVar [15] and RMBase v2.0 [16] databases also confirmed the presence of RRACH m^{6}A sequence motifs in PIK3R1. Consistently, CLIP and RIP data from the m^{6}A2Target database [17] identified PIK3R1 mRNA as a potential target of YTHDF1 (GSE78030 and GSE63591) on the exons as well as 3'UTR sites. After knocking down YTHDF1 expression in two HCC

cell lines (Fig. 7a), we found that PIK3R1 protein expression and the m^{6}A level of PIK3R1 were significantly reduced (Fig. 7b and c). In contrast, ectopic expression of YTHDF1 in HepG2 and Huh7 cell lines resulted in a remarkable increase in the protein expression and m^{6}A level of PIK3R1 (Fig. 7d-f). RT-qPCR analysis showed that YTHDF1 overexpression did not affect the mRNA level of PIK3R1 (Fig. 7g). YTHDF1 overexpression significantly elevated the presence of PIK3R1 mRNA in the polysome fraction (Fig. 7h). Moreover, introduction of YTHDF1 abolished the inhibitory effects of circRHBDD1 knockdown on PIK3R1 protein expression levels (Fig. 7i), but had no effects on PIK3R1 mRNA expression (Fig. 7j).

To elucidate whether YTHDF1-mediated PIK3R1 upregulation was dependent on m^{6}A modification, we generated a Flag-tagged mutant YTHDF1 construct (YTHDF1-Mut) with two point mutations (K395A and Y397A) to abrogate its m^{6}A-binding ability as previously reported [18, 19]. After YTHDF1 wide-type (YTHDF1-WT) and YTHDF1-Mut recombination plasmids were successfully transfected into HepG2 and Huh7 cells, we found that the elevated protein expression of PIK3R1 in YTHDF1-WT were abolished in YTHDF1-Mut transfected HCC cells (Fig. 7k). However, the PIK3R1 mRNA levels were comparable between YTHDF1-WT and YTHDF1-Mut (Fig. 7l). Ectopic expression of YTHDF1-Mut dramatically sabotaged the interaction between PIK3R1 mRNA and YTHDF1 according to the results of RIP assay (Fig. 7m). Collectively, the above data demonstrated that circRHBDD1 interacted with YTHDF1 to augment the translation of PIK3R1 mRNA in an m^{6}A-dependent manner.

In an attempt to map the YTHDF1-interacting region of circRHBDD1, we constructed three nonoverlapping biotinylated RNA fragments spanning the body of the circRNA (P1: 1-100 nt; P2: 101-200 nt; P3: 201-290 nt), as illustrated in Additional file 10: Fig. S6A. After incubating each biotinylated RNA with the cell lysates, we performed pull-down assay followed by YTHDF1 western blotting analysis. As shown in Additional file 10: Fig. S6B, we observed specific binding of YTHDF1 to P1. Then, we determined which domain of YTHDF1 was necessary for the binding of YTHDF1 to circRHBDD1 using Flag-tagged full-length YTHDF1 and two truncated constructs (YTHDF1-N: N-terminus, 1-359 aa; YTHDF1-C: C-terminus, also known as the YTH domain, 360-559 aa). RIP assay revealed that the N-terminus of YTHDF1 mediated its interaction with circRHBDD1 (Additional file 10: Fig. S6C and D).

EIF4A3 promotes the expression of circRHBDD1

RNA-binding proteins can bind to the flanking intron sequences of circRNAs and mediate circRNA biogenesis [20]. To investigate the upstream regulator of circRHBDD1 in HCC, we searched CircInteractome database [21] and found three EIF4A3 binding sites flanking circRHBDD1, referred to as site a, b, and c (Fig. 8a). TCGA data showed that EIF4A3 was upregulated in HCC and high EIF4A3 expression was associated with poor overall survival (Fig. 8b and c). Previous studies showed that EIF4A3, as a key component of the exon junction complex, promotes the expression of several circRNAs [22-24]. Correlation analysis revealed that circRHBDD1 level was positively correlated to the expression level of EIF4A3 (Fig. 8d). In order to elucidate the effect of EIF4A3 on circRHBDD1 expression, we knocked down EIF4A3 expression using two siRNAs in both HCCLM3 and MHCC97H cells (Fig. 8e and f). As indicated in Fig. 8g, circRHBDD1 level was significantly decreased after EIF4A3 knockdown. Similarly,

overexpression of EIF4A3 led to an increase in circRHBDD1 expression level in HepG2 and Huh7 cells (Fig. 8h-j). In contrast, both the mRNA and protein levels of EIF4A3 were not altered in circRHBDD1-silenced cells (Additional file 11: Fig. S7A and B). Fig. 8k indicated that EIF4A3 could bind to the flanking sequences through two upstream putative binding sites (site a and b), but not the downstream site (site c). Mutant of both site a and b abolished the reduction of circRHBDD1 expression level in EIF4A3-silenced cells (Fig. 8l). These results demonstrated that EIF4A3 might induce the biogenesis of circRHBDD1 via binding to site a and b. Taken together, we demonstrated that EIF4A3-mediated upregulation of circRHBDD1 could interact with YTHDF1 to promote PIK3R1 translation in an m^6A-dependent manner, consequently activating the PI3K/AKT signaling and facilitating glycolysis and glutaminolysis in HCC.

CircRHBDD1 restricts anti-PD-1 therapy in HCC

Targeting of cancer metabolism, and thus the associated reprogramming of the tumor microenvironment, can unleash anti-tumor immune responses. Inhibitors of glycolysis as well as glutaminolysis can induce synergistic responses with immunotherapy [25]. Given that circRHBDD1 could augment HCC glycolysis and glutaminolysis, we next evaluated whether circRHBDD1 inhibition could enhance the efficacy of anti-PD-1 therapy in HCC. We analyzed 18 HCC patients with recurrence or distant metastasis receiving anti-PD-1 therapy. After four cycles of anti-PD-1 treatment, the efficacy was assessed using CT or MRI. There were three patients with partial response, two patients with stable disease, and 13 patients with progressive disease, as defined by RECIST1.1 (Additional file 12: Fig. S8). Patients were classified into the responder group (partial response and stable disease) or the non-responder group (progressive disease) [26, 27]. As shown in Fig. 9a, the expression level of circRHBDD1 in the non-responder group was much higher than that in the responder group. To further delineate the effects of circRHBDD1 on the efficacy of anti-PD1 therapy, we established a xenograft model by subcutaneous implantation of circRHBDD1-silenced Hepa1-6 cells or control cells and were subjected to anti-PD-1 or IgG treatment (Fig. 9b and Additional file 13: Fig. S9). Treatment of immunocompetent mice harboring circRHBDD1-silenced tumors with anti-PD-1 significantly hindered tumor growth and improved mouse overall survival (Fig. 9c-e). A schematic diagram for the functions and mechanisms of circRHBDD1 in HCC is concluded in Fig. 9f.

Discussion

Benefitted from the rapid development and application of high-throughput sequencing technology, emerging studies have identified abnormal expression patterns of circRNAs in different human cancers. The involvement of circRNAs in metabolic reprogramming of HCC cells, however, remains unclear. Here, we reported that a RHBDD1-derived circRNA participated in the glucose and glutamine metabolic alternations and cancer immunotherapy in HCC. We employed two independent HCC cohorts and demonstrated that circRHBDD1 was highly expressed in HCC tissues and correlated to unfavorable clinicopathological features. Univariate and multivariate survival analyses revealed that high circRHBDD1 expression was an independent predictive factor for overall survival and disease-free survival in HCC patients.

Cancer cells tend to accumulate metabolic alternations to acquire necessary nutrients to promote growth and survival [28]. Glucose as well as amino acid metabolism is frequently hijacked by tumor cells to maintain viability and build new biomass. Emerging evidence has revealed the regulatory roles of circRNAs in cancer cell glycolysis and glutamine metabolism [29]. In colorectal cancer, circACC1 modulates glycolysis through promoting the enzymatic activity of the AMPK holoenzyme [30]. CircHMGCS1 promotes hepatoblastoma cell proliferation, apoptosis, and glutamine metabolism through serving as a microRNA sponge [31]. In this study, the results from RNA-seq and pathway enrichment analysis suggested the potential involvement of circRHBDD1 in glucose and glutamine metabolic alternations in HCC. Utilizing loss-of-function and gain-of-function assays, we examined the effects of circRHBDD1 on ECAR, OCR, as well as the levels of several key transporters, enzymes, and metabolites in glycolysis and glutaminolysis. The results demonstrated that circRHBDD1 was closely associated with the augmented glycolysis and glutaminolysis of HCC cells. Recapitulating the principal morphologic and genetic features of the original tumors, PDX models represent powerful resources for evaluating the *in vivo* effect of novel therapeutic strategies [32]. In consistence with the *in vitro* results, we constructed PDX mouse models and verified the tumor-promoting effects of circRHBDD1 *in vivo*.

The PI3K/AKT signaling pathway orchestrates multiple metabolic processes in cancer, and plays an important role in the regulation of glucose and glutamine metabolism. As a regulatory subunit of PI3K, PIK3R1 activates the PI3K/AKT signaling to accelerate the processes of glycolysis and glutaminolysis [33]. In breast cancer, miR-155-mediated PIK3R1 upregulation positively modulates glucose metabolism through FOXO3a/cMYC axis [34]. It has also been reported that PIK3R1 facilitates glutaminolysis to promote gastric cancer progression [35]. Herein, we demonstrated that circRHBDD1 activated the PI3K/AKT signaling through PIK3R1. CircRHBDD1 upregulation led to elevated protein levels of PIK3R1, and circRHBDD1 knockdown resulted in the opposite results. However, no statistically significant change in PIK3R1 mRNA was observed upon circRHBDD1 overexpression or knockdown. Treatment of MG132 or CQ could not reverse the decreased PIK3R1 protein levels in circRHBDD1-silenced HCC cells, indicating that circRHBDD1 did not affect the degradation of PIK3R1 protein. Polysome profiling analysis revealed that circRHBDD1 facilitated PIK3R1 protein expression possibly via translational control.

As the most abundant posttranscriptional mRNA modification, m^6A is involved in numerous biological processes. Dynamic and reversible m^6A modification is installed by m^6A methyltransferases (writers), recognized by m^6A-binding proteins (readers), and removed by demethylases (erasers). M^6A participates in almost every aspect of the RNA life cycle, including mRNA translation, splicing, and stabilization [36]. In order to elucidate how circRHBDD1 regulated the translation of PIK3R1, we performed RNA pull-down assay followed by mass spectrometry and YTHDF1 was demonstrated to interact with circRHBDD1. As an m^6A reader protein, YTHDF1 recognizes the m^6A sites and promotes the targeted mRNA translation [37]. Reportedly, YTHDF1 augments EIF3C translation in an m^6A-dependent manner, thereby facilitating ovarian cancer tumorigenesis and metastasis [13]. Recruitment of YTHDF1 to m^6A-modified TRIM29 participates in the translation of TRIM29 in cisplatin-resistant ovarian cancer cells [38]. The translation of FZD7 is controlled by YTHDF1 in gastric carcinogenesis [19]. In the present study, we combined four

bioinformatics databases and meRIP assays, and found that YTHDF1 promoted PIK3R1 mRNA translation via m[6]A modification. Functional deletion of YTH domain blocks the m[6]A-binding capability of YTHDF1. Here in our study, we found that YTHDF1-Mut interrupted the interaction between PIK3R1 mRNA and YTHDF1, and abolished the increased expression levels of PIK3R1 protein in HCC cells. The involvement of other m[6]A writers and erasers in the interaction between YTHDF1 and PIK3R1 still needs further investigation.

RNA-binding proteins have been proposed to function as *trans* factors in the regulation of circRNA biogenesis. Reportedly, QKI could enhance circRNA formation by binding to the introns flanking circRNA-forming exons, and bring the circularized exons closer together. Splicing factors, including EIF4A3, FUS, HNRNPL, RBM20, and Mbl, have been found to modulate circRNA generation in different biological settings [39]. In the present study, we found that EIF4A3 could bind to the upstream region of the RHBDD1 pre-mRNA transcript and regulate the expression of circRHBDD1. EIF4A3-mediated exon back-splicing could be responsible for the upregulation of circRHBDD1 in HCC.

An impressive clinical benefit has been observed in a fraction of HCC patients treated with PD-1 checkpoint blockade. However, limited response to anti-PD-1 therapy in most patients remains a major challenge. Cancer cell metabolic reprogramming modulates the tumor microenvironment [40]. Glycolytic activity of cancer cells promotes the secretion of lactate and acidification of the tumor milieu, which compromises the anti-tumor immune response of T and NK cells [41]. Reportedly, aerobic glycolytic activity in human tumors is negatively associated with the efficacy of immunotherapy [42]. CB-839, an allosteric inhibitor of GLS, effectively inhibits glutaminolysis and has been shown to synergize with PD-1 inhibitors in anticancer immunotherapy [43]. In this study, we demonstrated that combination of circRHBDD1 inhibition and anti-PD-1 treatment could achieve a better anti-tumor efficacy. These results suggested that circRHBDD1 could be a potential therapeutic candidate, alone or in combination with immune checkpoint blockade, for HCC.

Conclusion

In summary, our findings indicated that circRHBDD1 expression was significantly elevated in HCC and promoted glycolysis and glutaminolysis of HCC cells. Mechanistically, circRHBDD1 interacted with YTHDF1 and augmented PIK3R1 translation in an m[6]A-dependent manner. EIF4A3 might induce the upregulation of circRHBDD1 in HCC. Furthermore, circRHBDD1 inhibition can synergize with anti-PD-1 therapy. Therefore, targeting the circRHBDD1/YTHDF1/PIK3R1 axis may hold promise for HCC therapeutic modality.

Abbreviations

HCC: Hepatocellular carcinoma; circRNA: Circular RNA; α-KG: α-ketoglutarate; PDX: Patient-derived xenograft; m[6]A: N[6]-methyladenosine; TMA: Tissue microarray; RT-qPCR: Quantitative real-time polymerase chain reaction; FISH: Fluorescence *in situ* hybridization; ISH: *In situ* hybridization; ECAR:

Extracellular acidification rate; OCR: Oxygen consumption rate; 2-DG, 2-deoxyglucose; FCCP: Carbonyl cyanide p-trifluoromethoxy phenylhydrazone; G6P: Glucose-6-phosphate; RIP: RNA immunoprecipitation; meRIP: Methylated RNA immunoprecipitation; IHC: Immunohistochemistry; TNM: Tumor-node-metastasis; HR: Hazard ratio; CI: Confidence interval; CCK-8: Cell Counting Kit-8; EdU: 5-ethynyl-2'-deoxyuridine; CQ: Chloroquine.

Declarations

Authors' contributions

JC, ZQC, XHW, and XLZ conceived and designed the study. JC, ZQC, and YZ collected clinical samples. JC, ZQC, JGW, JFW, ZZZ, and HRL performed the experiments. JC, YZ, JDW, JDM, and XLZ analyzed the data. JC and ZQC wrote the paper. XHW, JDM, and XLZ revised the paper. All authors read and approved the final manuscript.

Availability of data and materials

All data generated or analyzed during this study are included in this article and its additional files. Supplementary methods, Figure S1 to S9, and Table S1 to S3 are attached as additional files.

Ethics approval and consent to participate

Patient tissue samples were obtained with informed consent, under the protocol approved by the Ethics Committee of the First Affiliated Hospital of Nanjing Medical University and the Ethics Committee of the First Affiliated Hospital of Wannan Medical College.

Consent for publication

Not applicable.

Competing interests

The authors declare that they have no competing interests.

Author details

[1]Department of Oncology, The First Affiliated Hospital, Yijishan Hospital of Wannan Medical College, Wuhu 241001, China. [2]Key Laboratory of Non-coding RNA Transformation Research of Anhui Higher Education Institution (Wannan Medical College), Wuhu 241001, China. [3]Hepatobiliary Center, The First Affiliated Hospital of Nanjing Medical University, Key Laboratory of Liver Transplantation, Chinese Academy of Medical Sciences, NHC Key Laboratory of Liver Transplantation, Nanjing 210029, China. [4]Department of Gastrointestinal Surgery, The First Affiliated Hospital, Yijishan Hospital of Wannan Medical College, Wuhu 241001, China. [5]State Key Laboratory of Reproductive Medicine, Nanjing Medical University, Nanjing 211166, China.
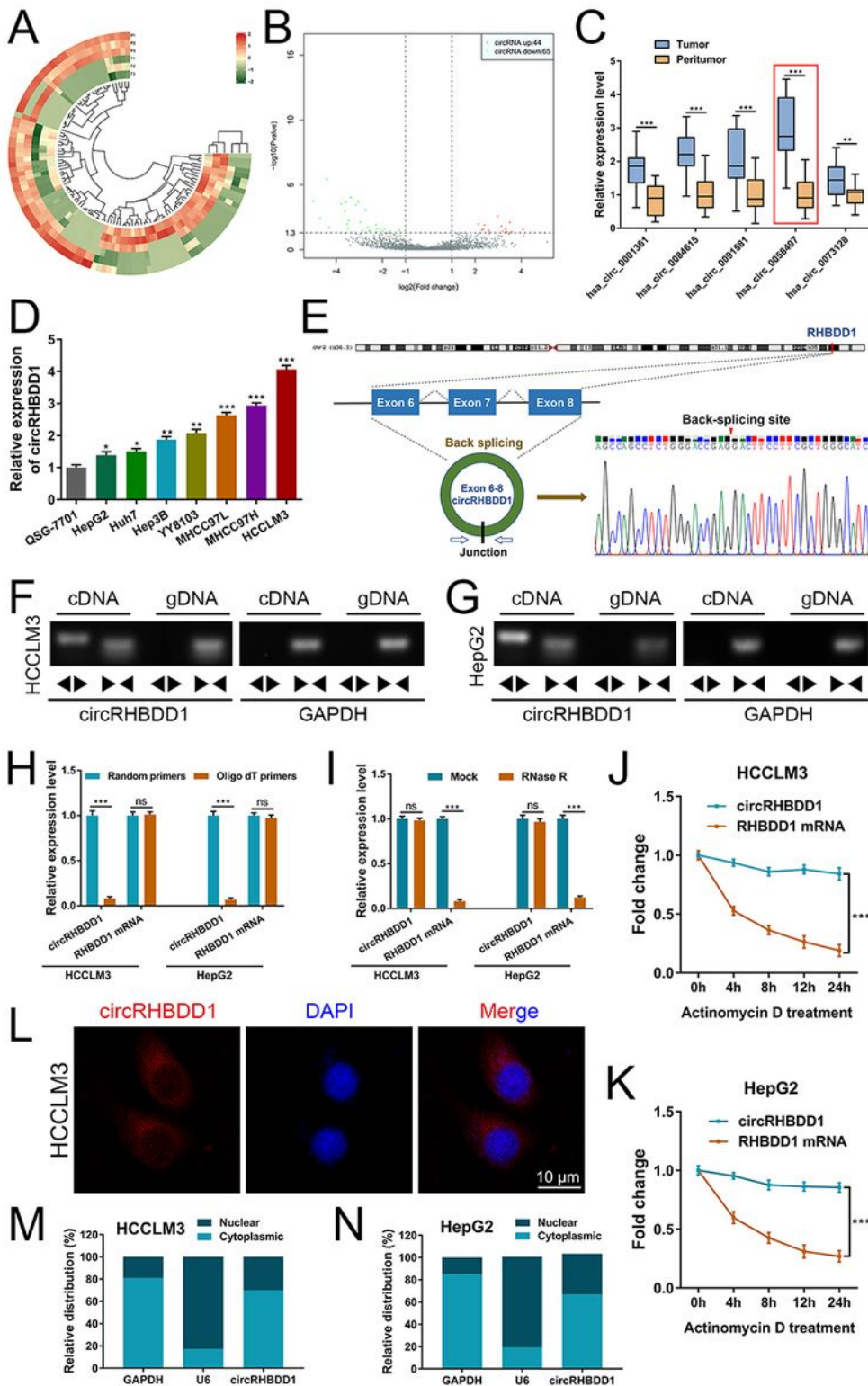
References

1. Sung H, Ferlay J, Siegel RL, Laversanne M, Soerjomataram I, Jemal A, Bray F. Global cancer statistics 2020: GLOBOCAN estimates of incidence and mortality worldwide for 36 cancers in 185 countries. CA Cancer J Clin. 2021. doi:10.3322/caac.21660.
2. Elia I, Haigis MC. Metabolites and the tumour microenvironment: from cellular mechanisms to systemic metabolism. Nat Metab. 2021;3(1):21–32.
3. Akins NS, Nielson TC, Le HV. Inhibition of glycolysis and glutaminolysis: an emerging drug discovery approach to combat cancer. Curr Top Med Chem. 2018;18(6):494–504.
4. Ma S, Kong S, Wang F, Ju S. CircRNAs: biogenesis, functions, and role in drug-resistant Tumours. Mol Cancer. 2020;19(1):119.
5. Li H, Yang F, Hu A, Wang X, Fang E, Chen Y, et al. Therapeutic targeting of circ-CUX1/EWSR1/MAZ axis inhibits glycolysis and neuroblastoma progression. EMBO Mol Med. 2019;11(12):e10835.
6. Cai J, Chen Z, Wang J, Wang J, Chen X, Liang L, et al. circHECTD1 facilitates glutaminolysis to promote gastric cancer progression by targeting miR-1256 and activating β-catenin/c-Myc signaling. Cell Death Dis. 2019;10(8):576.
7. Zuo X, Chen Z, Gao W, Zhang Y, Wang J, Wang J, et al. M6A-mediated upregulation of LINC00958 increases lipogenesis and acts as a nanotherapeutic target in hepatocellular carcinoma. J Hematol Oncol. 2020;13(1):5.
8. Zuo X, Chen Z, Cai J, Gao W, Zhang Y, Han G, et al. 5-hydroxytryptamine receptor 1D aggravates hepatocellular carcinoma progression through FoxO6 in AKT-dependent and independent manners. Hepatology. 2019;69(5):2031–47.
9. He S, Zhang J, Zhang W, Chen F, Luo R. FOXA1 inhibits hepatocellular carcinoma progression by suppressing PIK3R1 expression in male patients. J Exp Clin Cancer Res. 2017;36(1):175.

10. Zhao Z, Yang L, Fang S, Zheng L, Wu F, Chen W, et al. The effect of m6A methylation regulatory factors on the malignant progression and clinical prognosis of hepatocellular carcinoma. Front Oncol. 2020;10:1435.

11. Qu N, Qin S, Zhang X, Bo X, Liu Z, Tan C, et al. Multiple m(6)A RNA methylation modulators promote the malignant progression of hepatocellular carcinoma and affect its clinical prognosis. BMC Cancer. 2020;20(1):165.

12. Wang X, Zhao BS, Roundtree IA, Lu Z, Han D, Ma H, et al. N(6)-methyladenosine modulates messenger RNA translation efficiency. Cell. 2015;161(6):1388–99.

13. Liu T, Wei Q, Jin J, Luo Q, Liu Y, Yang Y, Cheng C, Li L, Pi J, Si Y, et al. The m6A reader YTHDF1 promotes ovarian cancer progression via augmenting EIF3C translation. Nucleic Acids Res. 2020;48(7):3816–31.

14. Liu S, Zhu A, He C, Chen M. REPIC: a database for exploring the N(6)-methyladenosine methylome. Genome Biol. 2020;21(1):100.

15. Luo X, Li H, Liang J, Zhao Q, Xie Y, Ren J, et al. RMVar: an updated database of functional variants involved in RNA modifications. Nucleic Acids Res. 2020;49(D1):D1405–12.

16. Xuan JJ, Sun WJ, Lin PH, Zhou KR, Liu S, Zheng LL, et al. RMBase v2.0: deciphering the map of RNA modifications from epitranscriptome sequencing data. Nucleic Acids Res. 2018;46(D1):D327–34.

17. Deng S, Zhang H, Zhu K, Li X, Ye Y, Li R, et al. M6A2Target: a comprehensive database for targets of m6A writers, erasers and readers. Brief Bioinform. 2020. doi:10.1093/bib/bbaa055.

18. Xu C, Liu K, Ahmed H, Loppnau P, Schapira M, Min J. Structural basis for the discriminative recognition of N6-methyladenosine RNA by the human YT521-B homology domain family of proteins. J Biol Chem. 2015;290(41):24902–13.

19. Pi J, Wang W, Ji M, Wang X, Wei X, Jin J, et al. YTHDF1 promotes gastric carcinogenesis by controlling translation of FZD7. Cancer Res. 2020. doi:10.1158/0008-5472.CAN-20-0066.

20. Kristensen LS, Andersen MS, Stagsted LVW, Ebbesen KK, Hansen TB, Kjems J. The biogenesis, biology and characterization of circular RNAs. Nat Rev Genet. 2019;20(11):675–91.

21. Dudekula DB, Panda AC, Grammatikakis I, De S, Abdelmohsen K, Gorospe M. CircInteractome. A web tool for exploring circular RNAs and their interacting proteins and microRNAs. RNA Biol. 2016;13(1):34–42.

22. Zheng X, Huang M, Xing L, Yang R, Wang X, Jiang R, et al. The circRNA circSEPT9 mediated by E2F1 and EIF4A3 facilitates the carcinogenesis and development of triple-negative breast cancer. Mol Cancer. 2020;19(1):73.

23. Wei Y, Lu C, Zhou P, Zhao L, Lyu X, Yin J, et al. EIF4A3-induced circular RNA ASAP1(circASAP1) promotes tumorigenesis and temozolomide resistance of glioblastoma via NRAS/MEK1/ERK1/2 signaling. Neuro Oncol. 2020. doi:10.1093/neuonc/noaa214.

24. Wang R, Zhang S, Chen X, Li N, Li J, Jia R, et al. EIF4A3-induced circular RNA MMP9 (circMMP9) acts as a sponge of miR-124 and promotes glioblastoma multiforme cell tumorigenesis. Mol Cancer. 2018;17(1):166.

25. Li X, Wenes M, Romero P, Huang SC, Fendt SM, Ho PC. Navigating metabolic pathways to enhance antitumour immunity and immunotherapy. Nat Rev Clin Oncol. 2019;16(7):425–41.

26. Aslan K, Turco V, Blobner J, Sonner JK, Liuzzi AR, Núñez NG, De Feo D, Kickingereder P, Fischer M, Green E, et al. Heterogeneity of response to immune checkpoint blockade in hypermutated experimental gliomas. Nat Commun. 2020;11(1):931.

27. Terranova-Barberio M, Pawlowska N, Dhawan M, Moasser M, Chien AJ, Melisko ME, Rugo H, Rahimi R, Deal T, Daud A, et al. Exhausted T cell signature predicts immunotherapy response in ER-positive breast cancer. Nat Commun. 2020;11(1):3584.

28. Pavlova NN, Thompson CB. The emerging hallmarks of cancer metabolism. Cell Metab. 2016;23(1):27–47.

29. Yu T, Wang Y, Fan Y, Fang N, Wang T, Xu T, Shu Y. CircRNAs in cancer metabolism: a review. J Hematol Oncol. 2019;12(1):90.

30. Li Q, Wang Y, Wu S, Zhou Z, Ding X, Shi R, Thorne RF, Zhang XD, Hu W, Wu M. CircACC1 regulates assembly and activation of AMPK complex under metabolic stress. Cell Metab. 2019;30(1):157–73.

31. Zhen N, Gu S, Ma J, Zhu J, Yin M, Xu M, Wang J, Huang N, Cui Z, Bian Z, et al. CircHMGCS1 promotes hepatoblastoma cell proliferation by regulating the IGF signaling pathway and glutaminolysis. Theranostics. 2019;9(3):900–19.

32. Invrea F, Rovito R, Torchiaro E, Petti C, Isella C, Medico E. Patient-derived xenografts (PDXs) as model systems for human cancer. Curr Opin Biotechnol. 2020;63:151–6.

33. Lee JH, Liu R, Li J, Wang Y, Tan L, Li XJ, Qian X, Zhang C, Xia Y, Xu D, et al. EGFR-phosphorylated platelet isoform of phosphofructokinase 1 promotes PI3K activation. Mol Cell. 2018;70(2):197–210.

34. Kim S, Lee E, Jung J, Lee JW, Kim HJ, Kim J, Yoo HJ, Lee HJ, Chae SY, Jeon SM, et al. microRNA-155 positively regulates glucose metabolism via PIK3R1-FOXO3a-cMYC axis in breast cancer. Oncogene. 2018;37(22):2982–91.

35. Li Q, Tian Y, Liang Y, Li C. CircHIPK3/miR-876-5p/PIK3R1 axis regulates regulation proliferation, migration, invasion, and glutaminolysis in gastric cancer cells. Cancer Cell Int. 2020;20:391.

36. Zhou Z, Lv J, Yu H, Han J, Yang X, Feng D, Wu Q, Yuan B, Lu Q, Yang H. Mechanism of RNA modification N6-methyladenosine in human cancer. Mol Cancer. 2020;19(1):104.

37. Lan Q, Liu PY, Haase J, Bell JL, Huttelmaier S, Liu T. The critical role of RNA m(6)A methylation in cancer. Cancer Res. 2019;79(7):1285–92.

38. Hao L, Wang JM, Liu BQ, Yan J, Li C, Jiang JY, Zhao FY, Qiao HY, Wang HQ. m6A-YTHDF1-mediated TRIM29 upregulation facilitates the stem cell-like phenotype of cisplatin-resistant ovarian cancer cells. Biochim Biophys Acta Mol Cell Res. 2020;1868(1):118878.

39. Li X, Yang L, Chen LL. The biogenesis, functions, and challenges of circular RNAs. Mol Cell. 2018;71(3):428–42.

40. Dey P, Kimmelman AC, DePinho RA. Metabolic codependencies in the tumor microenvironment. Cancer Discov. 2021. doi:10.1158/2159-8290.CD-20-1211.

41. Renner K, Bruss C, Schnell A, Koehl G, Becker HM, Fante M, et al. Restricting glycolysis preserves T cell effector functions and augments checkpoint therapy. Cell Rep. 2019;29(1):135–50.

42. Cascone T, McKenzie JA, Mbofung RM, Punt S, Wang Z, Xu C, Williams LJ, Wang Z, Bristow CA, Carugo A, et al. Increased tumor glycolysis characterizes immune resistance to adoptive T cell therapy. Cell Metab. 2018;27(5):977–87.

43. Tannir NM, Motzer RJ, Agarwal N, Liu PY, Escudier B. CANTATA. A randomized phase 2 study of CB-839 in combination with cabozantinib vs. placebo with cabozantinib in patients with advanced/metastatic renal cell carcinoma. J Clin Oncol. 2018;36(15_suppl):TPS4601.

Figures

Figure 1

CircRHBDD1 is highly expressed in HCC. a Cluster heat map showing the differentially expressed circRNAs in paired human HCC tissues and peritumor tissues (n = 3). b Volcano plot showing circRNAs that changed significantly between HCC tissues and matched peritumor tissues. A total of 44 and 65 circRNAs were upregulated and downregulated in HCC tissues, respectively. c Expression levels of the five most upregulated circRNAs were validated by RT-qPCR in 20 matched HCC and peritumor tissues from

cohort 1. d Expression levels of circRHBDD1 in seven human HCC cell lines along with the normal human liver cell line QSG-7701. e Structure and back-splicing site of circRHBDD1. f and g CircRHBDD1 and GAPDH were amplified from cDNA or gDNA from HCCLM3 and HepG2 cells with divergent and convergent primers, respectively. h RT-qPCR assay for circRHBDD1 and RHBDD1 mRNA using the template cDNA reverse-transcribed by random primers and oligo dT primers in HCCLM3 and HepG2 cells. i RT-qPCR analysis for the expression of circRHBDD1 and RHBDD1 mRNA in HCCLM3 and HepG2 cells treated with RNase R. j and k RT-qPCR assay for the expression of circRHBDD1 and RHBDD1 mRNA in HCCLM3 and HepG2 cells treated with the transcription inhibitor actinomycin D at the indicated time points. l FISH detection of circRHBDD1 in HCCLM3 cells. m and n Abundance of circRHBDD1 from separated nuclear and cytoplasmic fractions was determined by RT-qPCR in HCCLM3 and HepG2 cells. * P < 0.05; ** P < 0.01; *** P < 0.001; ns, no significance.

Figure 2

CircRHBDD1 predicts unfavorable patient survival in HCC. a Expression levels of circRHBDD1 in 96 paired HCC and peritumor tissues from cohort 1 were determined by RT-qPCR (P < 0.001). b FISH detection of circRHBDD1 in 10 matched HCC and peritumor tissues from cohort 1. c Expression levels of circRHBDD1 were compared between patients with tumor size ≤ 5 cm and those with tumor size > 5 cm. d CircRHBDD1 expression levels were detected between the TNM stage I-II group and the TNM III-IV group. e

Expression levels of circRHBDD1 were measured by in situ hybridization (ISH) staining using tissue microarrays (n = 160). ISH intensity scores were defined as follows: 0 (weak), 1 (moderate), 2 (strong), and 3 (very strong). The staining intensity criteria was demonstrated on the right panel. The 100 dots shown in the left panel represent the percentage of tissues. f Kaplan-Meier analysis of the correlation between circRHBDD1 expression levels and overall survival (P < 0.001). g Multivariate analyses of the independent predictive factors for overall survival. Hazard ratios (HRs) and the corresponding 95% confidence intervals (CIs) are shown. h Kaplan-Meier analysis of the association of circRHBDD1 expression levels with disease-free survival (P < 0.001). i Multivariate analyses of the independent predictive factors for disease-free survival. HRs with the corresponding 95% CIs are shown. ***P < 0.001.
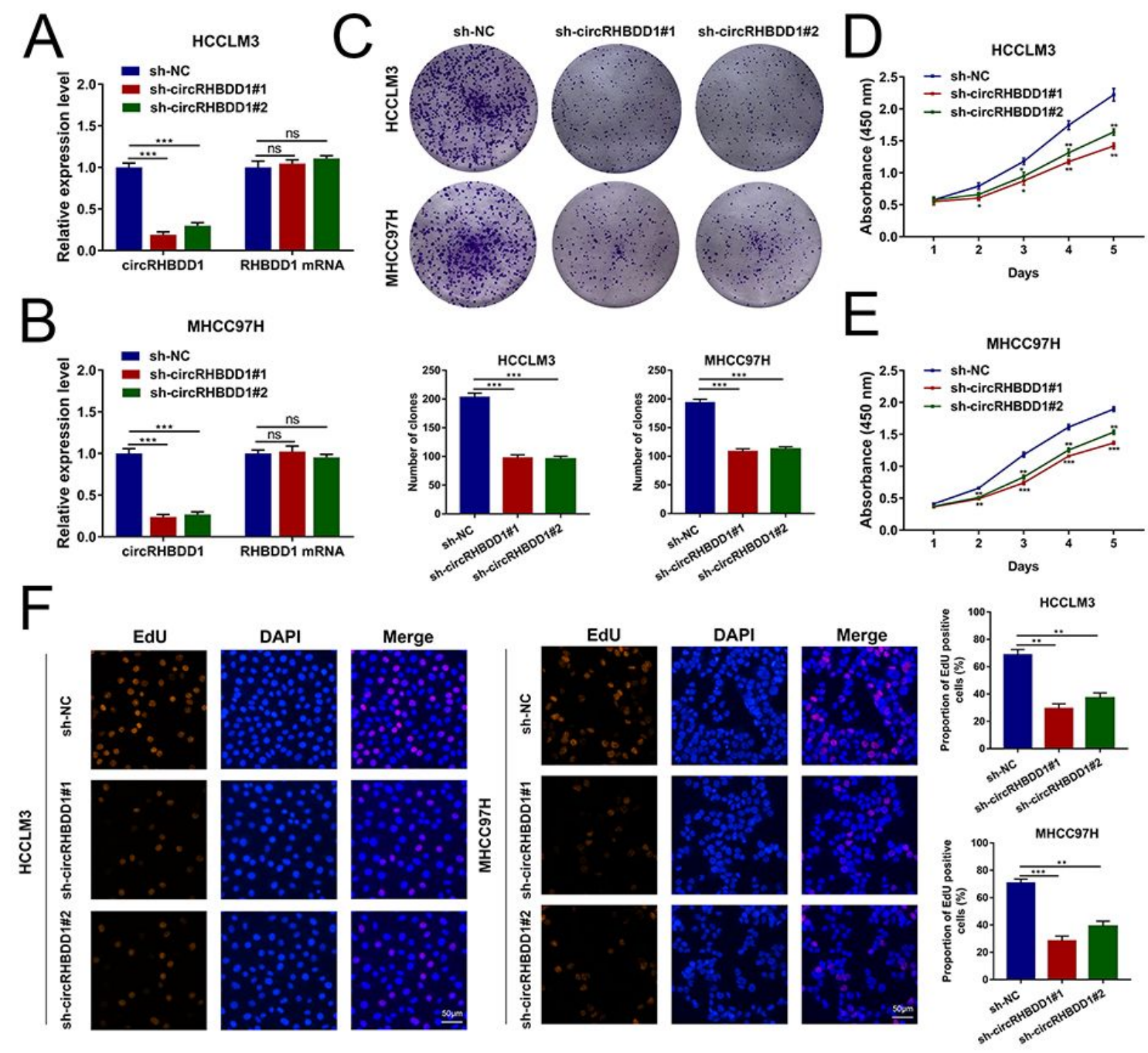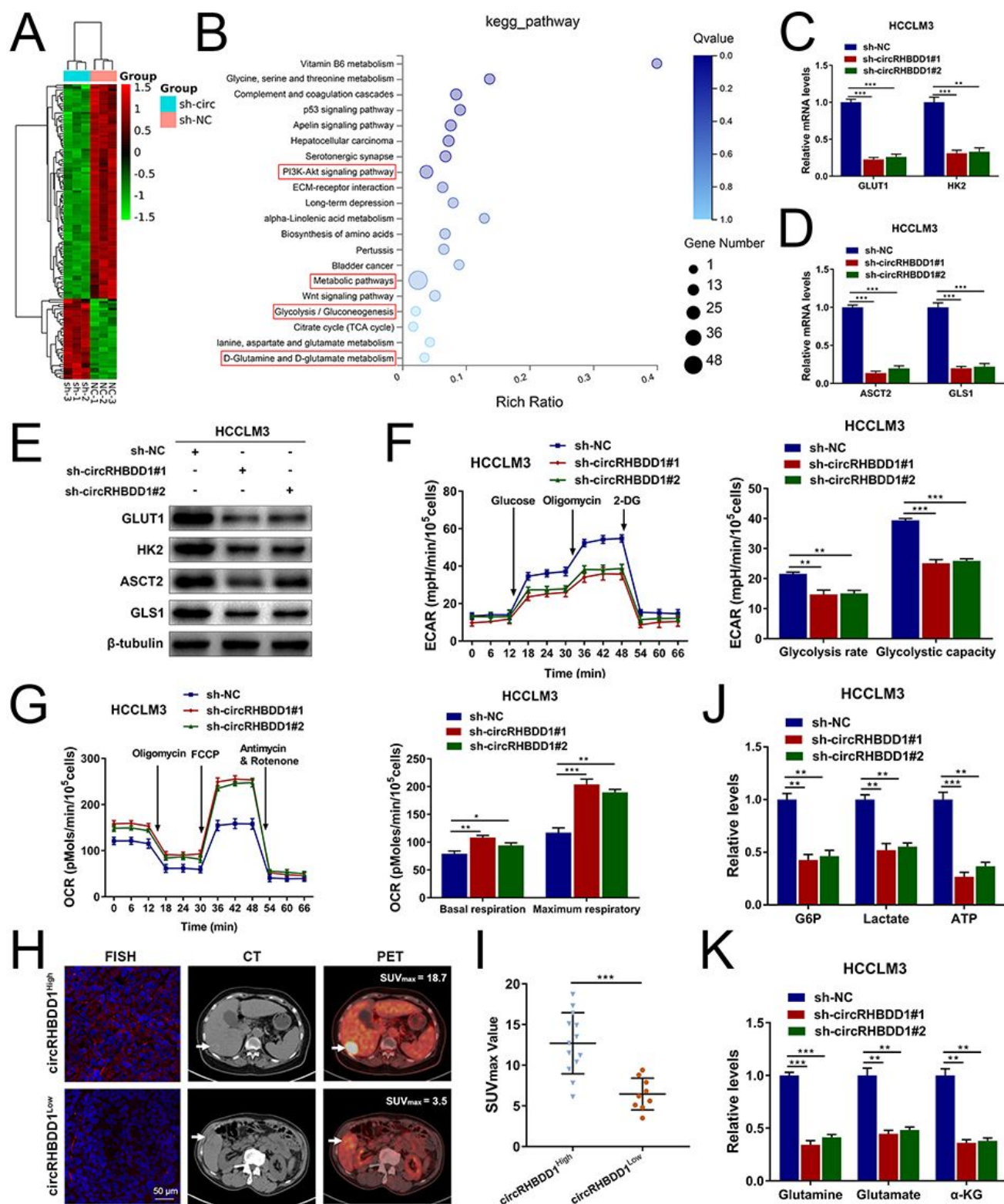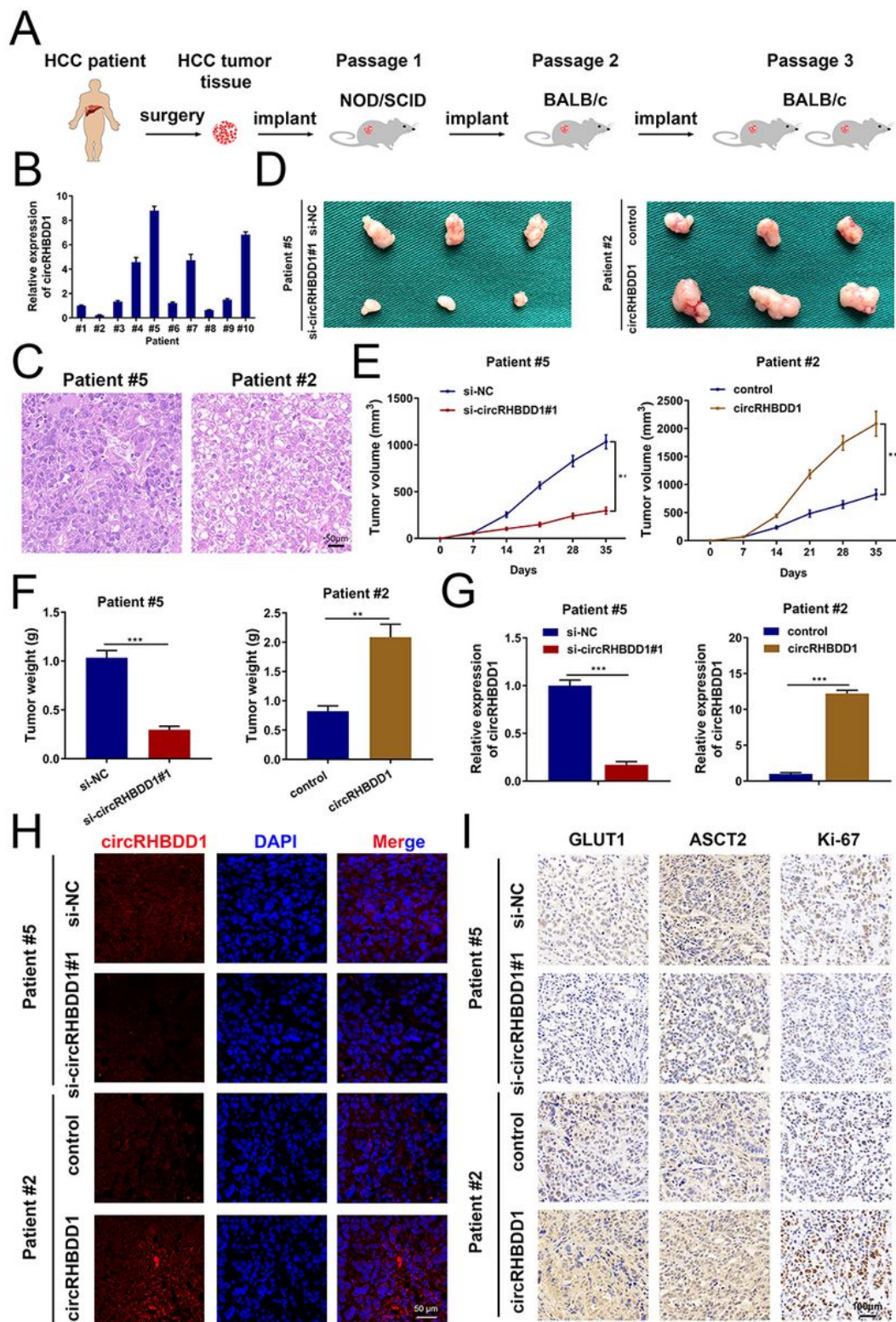

Figure 3

Knockdown of circRHBDD1 inhibits HCC viability in vitro. a RT-qPCR analysis of circRHBDD1 and RHBDD1 mRNA in HCCLM3 cells after the transfection of two shRNAs targeting the back-spliced sequence of circRHBDD1. b RT-qPCR analysis of circRHBDD1 and RHBDD1 mRNA in MHCC97H cells after the transfection of sh-circRHBDD1#1 and sh-circRHBDD1#2. c Proliferation ability was evaluated by colony formation assay (representative wells are presented) in circRHBDD1-silenced HCCLM3 and MHCC97H cells. d The proliferation of HCCLM3 cells after circRHBDD1 silencing was detected by CCK-8 assay. e The proliferation of circRHBDD1-silenced MHCC97H cells was examined using CCK-8 assay. f EdU assays were conducted to assess the proliferative ability of HCCLM3 and MHCC97H cells with circRHBDD1 knockdown. * $P < 0.05$; ** $P < 0.01$; *** $P < 0.001$; ns, no significance.

Figure 4

CircRHBDD1 knockdown suppresses glycolysis and glutaminolysis in HCCLM3 cells. a Heatmap showing the differentially expressed genes upon circRHBDD1 knockdown in HCCLM3 cells (n = 3). b KEGG pathway enrichment analysis showing the top canonical pathways after circRHBDD1 knockdown. c The expression levels of GLUT1 and HK2 mRNA were determined by RT-qPCR in circRHBDD1-silenced HCCLM3 cells. d The mRNA levels of ASCT2 and GLS1 were assessed using RT-qPCR in HCCLM3 cells

with circRHBDD1 knockdown. e Western blotting analysis was performed to detect the expression levels of GLUT1, HK2, ASCT2, and GLS1 in circRHBDD1-silenced HCCLM3 cells. f The ECAR data showed that silencing circRHBDD1 significantly reduced the rate of glycolysis and the glycolytic capacity in HCCLM3 cells. g The OCR results showed that circRHBDD1-silenced HCCLM3 cells displayed increased basal respiration and maximum respiratory. h FISH was used to determine the expression of circRHBDD1. Representative 18F-FDG PET/CT imaging of HCC patients with high or low circRHBDD1 expression is shown. i Analysis of SUVmax in the circRHBDDhigh and circRHBDDlow groups (n = 22). j The cellular G6P level, lactate production, and cellular ATP level were detected in HCCLM3 cells with circRHBDD1 knockdown. k The levels of glutamine, glutamate, and α-KG were examined in circRHBDD1-silenced HCCLM3 cells. * $P < 0.05$; ** $P < 0.01$; *** $P < 0.001$.

Figure 5

CircRHBDD1 facilitates HCC tumor growth in vivo. a A graphic illustration of the establishment of HCC PDX mouse models. b Expression levels of circRHBDD1 were detected in the xenografts isolated from mice of PDX using RT-qPCR. The engrafted tumors derived from patient #5 had the highest expression level of circRHBDD1, whereas the xenografts originating from patient #2 exhibited the lowest circRHBDD1 level. c The engrafted tumors from patient #5 and patient #2 were histopathologically

analyzed. d Photographs of the engrafted tumors from PDX mice treated with circRHBDD1 plasmid or cholesterol-conjugated circRHBDD1 siRNA. e Tumor volume was measured in the engrafted tumors. f Tumor weight was recorded in the engrafted tumors. g Expression levels of circRHBDD1 were detected in the engrafted tumors by RT-qPCR. h FISH images showing the expression levels of circRHBDD1 in the engrafted tumors. i Expression levels of GLUT1, ASCT2, and Ki-67 in the tumor tissues of PDX were analyzed using immunohistochemistry. * P < 0.05; ** P < 0.01; *** P < 0.001.
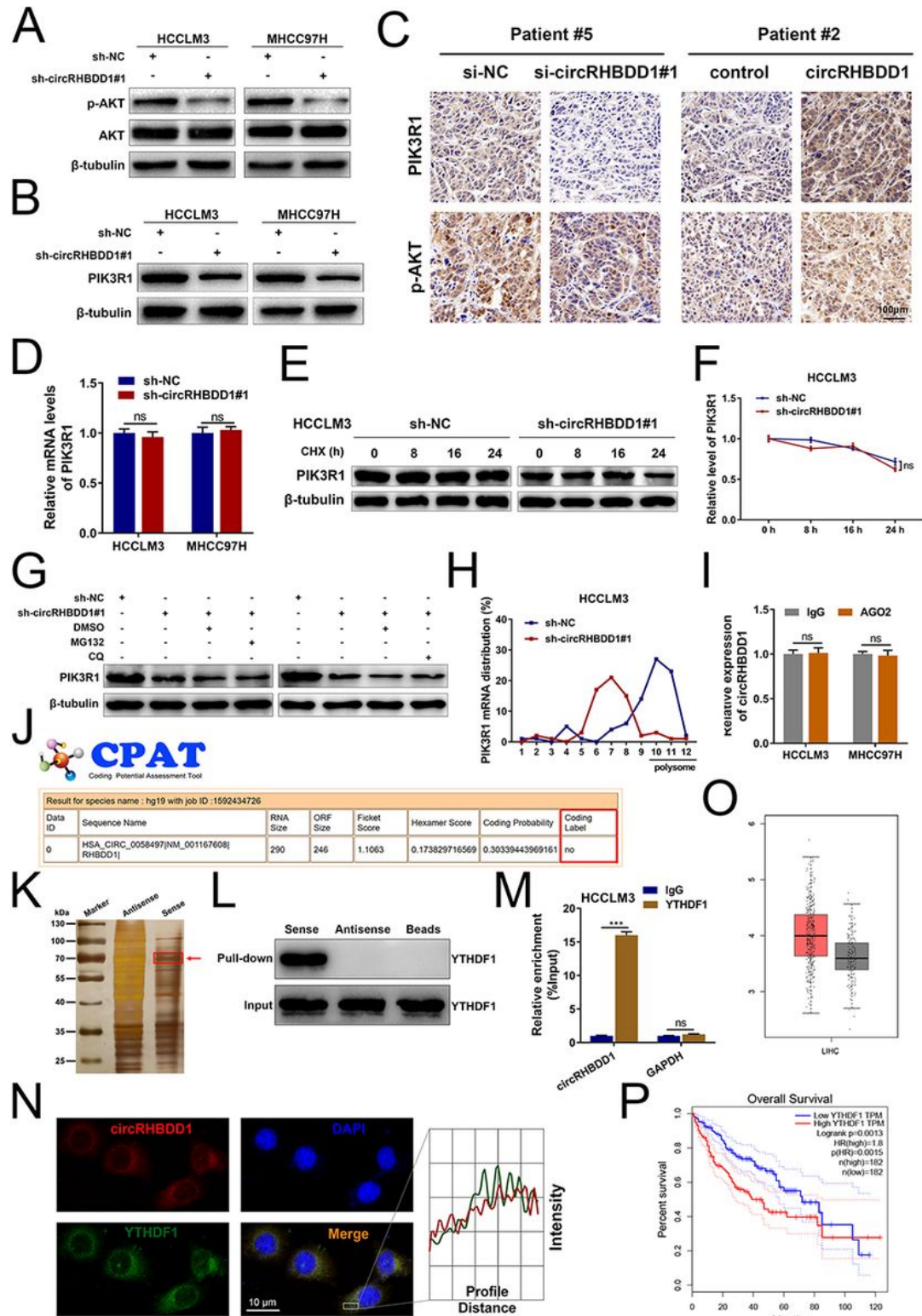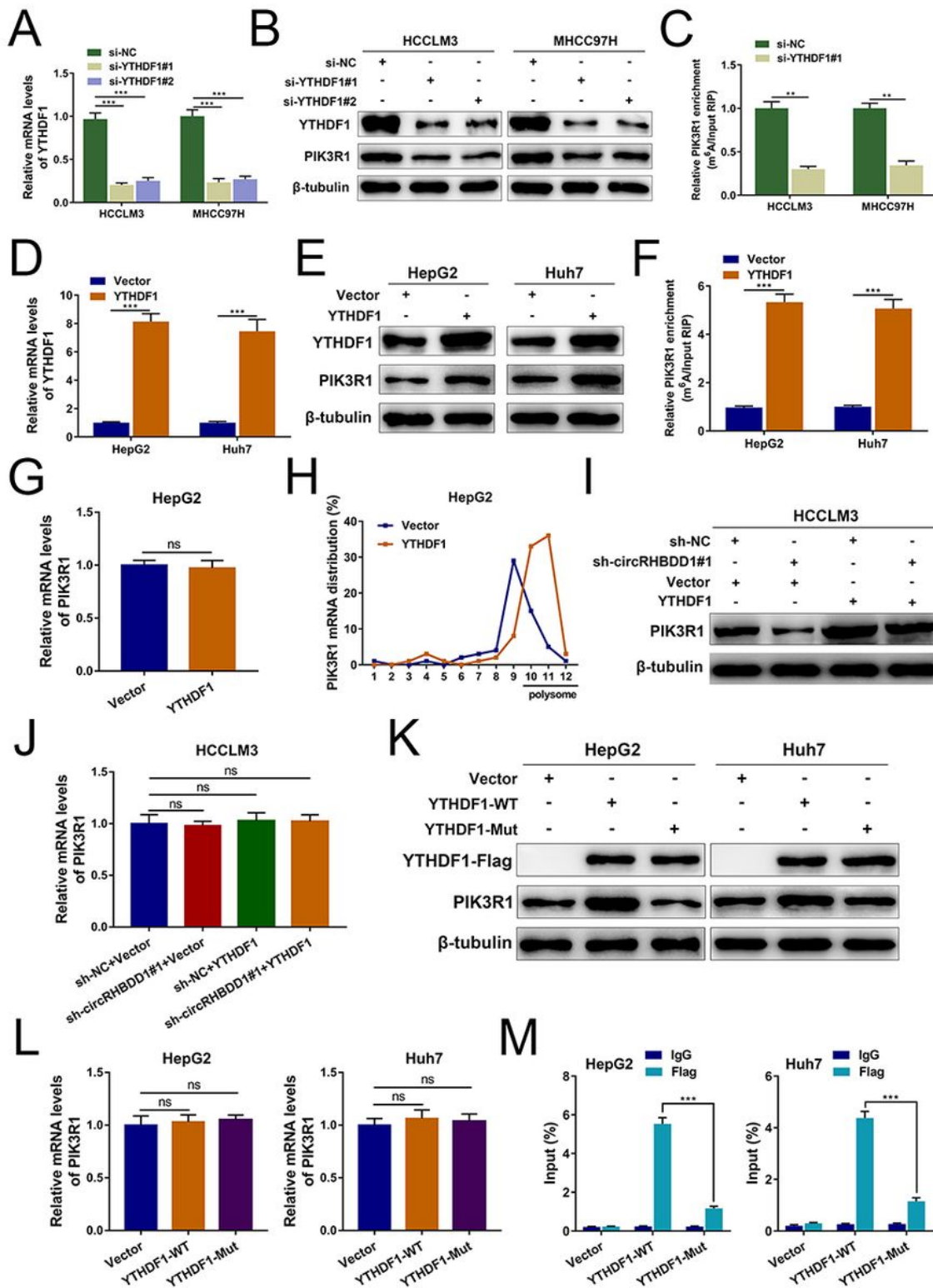

Figure 6

CircRHBDD1 activates the PI3K/AKT signaling via augmenting YTHDF1-mediated translation of PIK3R1. a Western blotting analysis showing the expression levels of p-AKT and AKT in circRHBDD1-silenced HCCLM3 and MHCC97H cells. b Expression levels of PIK3R1 in circRHBDD1-silenced HCCLM3 and MHCC97H cells were determined by western blotting. c Expression levels of PIK3R1 and p-AKT in the tumor tissues of PDX were analyzed using immunohistochemistry. d PIK3R1 mRNA levels were detected by RT-qPCR in circRHBDD1-silenced HCCLM3 and MHCC97H cells. e and f The effects of circRHBDD1 knockdown on the degradation of PIK3R1 protein in HCCLM3 cells pretreated with cycloheximide (CHX) were analyzed by western blotting analysis. g The effects of MG132 and chloroquine (CQ) on circRHBDD1 knockdown-induced PIK3R1 downregulation were determined by western blotting analysis. h Amount of PIK3R1 mRNA in various polysome fractions was analyzed by RT-qPCR. i AGO2-RIP assay was performed to detect the levels of circRHBDD1 in the AGO2 IP pellet. j Results from CPAT database indicating the absence of coding potential for circRHBDD1. k Identification of the circRHBDD1-protein complex pulled down by circRHBDD1 probe with protein extracts from HCCLM3 cells. This was followed by mass spectrometry. The arrows indicating the YTHDF1 band presented in circRHBDD1-protein complex. l RNA pull-down assay followed by western blotting for YTHDF1 in HCCLM3 cells. m The interaction between YTHDF1 and circRHBDD1 was verified by RIP assay. n FISH for circRHBDD1 and immunofluorescence for YTHDF1 in HCCLM3 cells. The profiles of colocalization are also provided. o TCGA data suggested that the expression level of YTHDF1 was upregulated in HCC tissues compared with the peritumor tissues ($P < 0.05$). p YTHDF1 was associated with unfavorable overall survival in HCC patients based on TCGA data (Hazard ratio = 1.8, $P = 0.0013$). *** $P < 0.001$; ns, no significance.
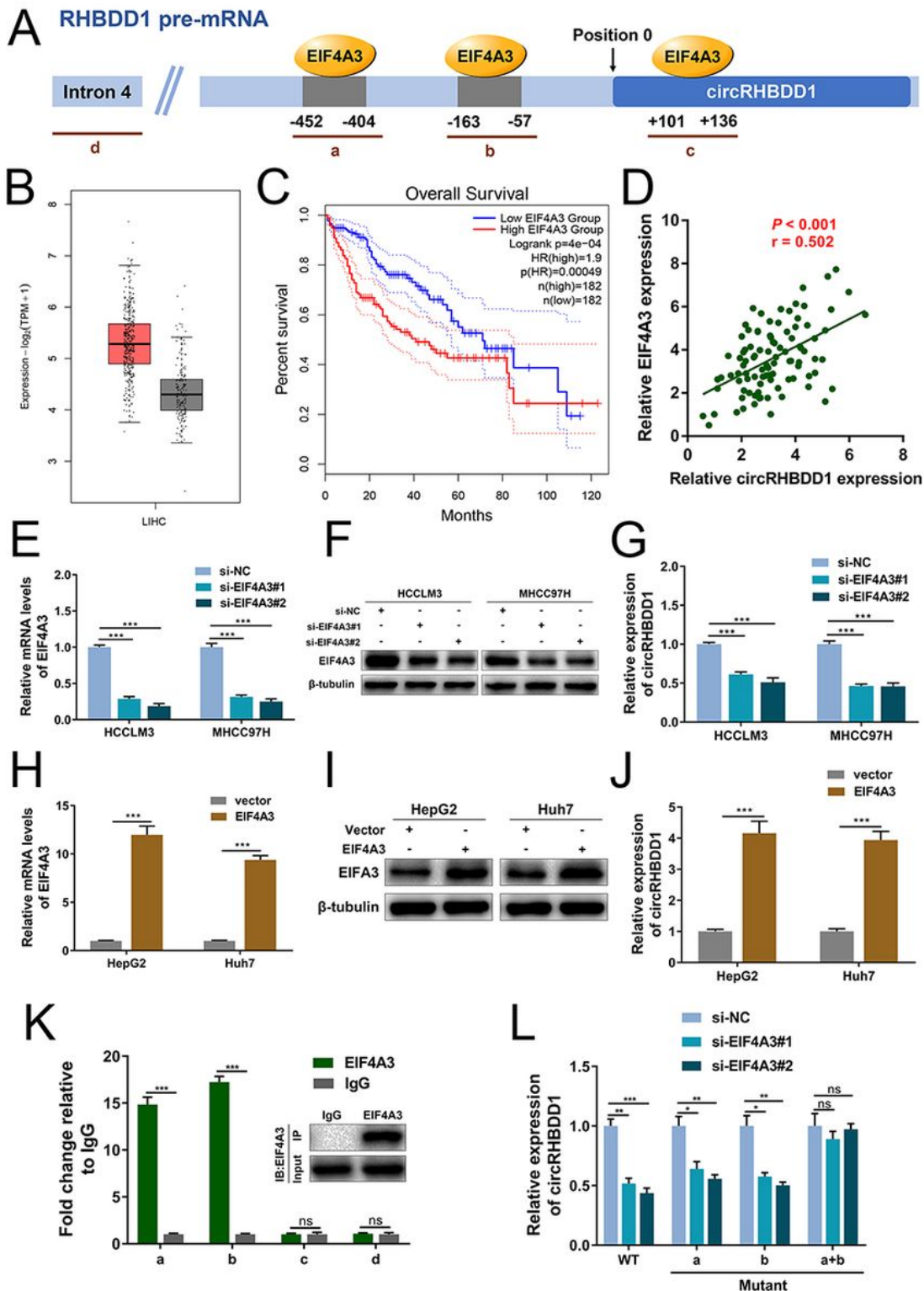
Figure 7

YTHDF1 regulates PIK3R1 translation in an m6A-dependent manner. a The knockdown efficiency of YTHDF1 siRNAs was validated by RT-qPCR in HCCLM3 and MHCC97H cells. b Western blotting assay showing the protein levels of YTHDF1 and PIK3R1 in YTHDF1-silenced HCCLM3 and MHCC97H cells. c MeRIP-qPCR analysis showing the m6A level of PIK3R1 detected in YTHDF1-silenced HCCLM3 and MHCC97H cells. d The overexpression efficiency of YTHDF1 plasmid was validated by RT-qPCR in HepG2

and Huh7 cells. e Western blotting assay showing the protein levels of YTHDF1 and PIK3R1 in YTHDF1-overexpressing HepG2 and Huh7 cells. f MeRIP-qPCR analysis showing the m6A level of PIK3R1 detected in YTHDF1-overexpressing HepG2 and Huh7 cells. g PIK3R1 mRNA levels of HepG2 cells with or without YTHDF1 overexpression were examined using RT-qPCR. h Amount of PIK3R1 mRNA in various polysome fractions was analyzed by RT-qPCR in HepG2 cells with or without YTHDF1 overexpression. i Western blotting analysis showing the expression levels of PIK3R1 in circRHBDD1-silenced HCCLM3 cells after YTHDF1 overexpression. j RT-qPCR analysis showing the mRNA levels of PIK3R1 in circRHBDD1-silenced HCCLM3 cells after YTHDF1 overexpression. k The protein levels of PIK3R1 in HepG2 and Huh7 cells transfected with YTHDF1 wild-type (WT) or mutant (Mut). l RT-qPCR analysis showing the mRNA levels of PIK3R1 in HepG2 and Huh7 cells transfected with YTHDF1-WT or YTHDF1-Mut. m PIK3R1-specific qPCR analysis of the co-precipitated RNAs by Flag antibody in RIP analysis. ** P < 0.01; *** P < 0.001; ns, no significance.

Figure 8

EIF4A3 promotes the expression of circRHBDD1. a The putative binding sites (site a, b, and c) of EIF4A3 in the upstream and downstream regions of RHBDD1 pre-mRNA were predicted with circInteractome database. b TCGA data suggested that the expression level of EIF4A3 was upregulated in HCC tissues compared with the peritumor tissues (P < 0.05). c EIF4A3 was associated with unfavorable overall survival in HCC patients based on TCGA data (Hazard ratio = 1.9, P = 0.0004). d Correlation analysis

revealed that circRHBDD1 level was positively correlated to the expression level of EIF4A3 in HCC tissues from cohort 1 (P < 0.001, r = 0.502). e The knockdown efficiency of EIF4A3 siRNAs was validated by RT-qPCR in HCCLM3 and MHCC97H cells. f Western blotting assay verifying the knockdown efficiency of EIF4A3 in HCCLM3 and MHCC97H cells. g The expression levels of circRHBDD1 in HCCLM3 and MHCC97H cells with EIF4A3 knockdown. h The overexpression efficiency of EIF4A3 was validated by RT-qPCR in HepG2 and Huh7 cells. i Western blotting assay verifying the overexpression efficiency of EIF4A3 in HepG2 and Huh7 cells. j The expression levels of circRHBDD1 in EIF4A3-overexpressing HepG2 and Huh7 cells. k RIP assay confirmed that EIF4A3 could directly bind to the RHBDD1 pre-mRNA at site a and b. l Mutant of both site a and b restored the reduction of circRHBDD1 expression level in EIF4A3-silenced cells. * P < 0.05; ** P < 0.01; *** P < 0.001; ns, no significance.
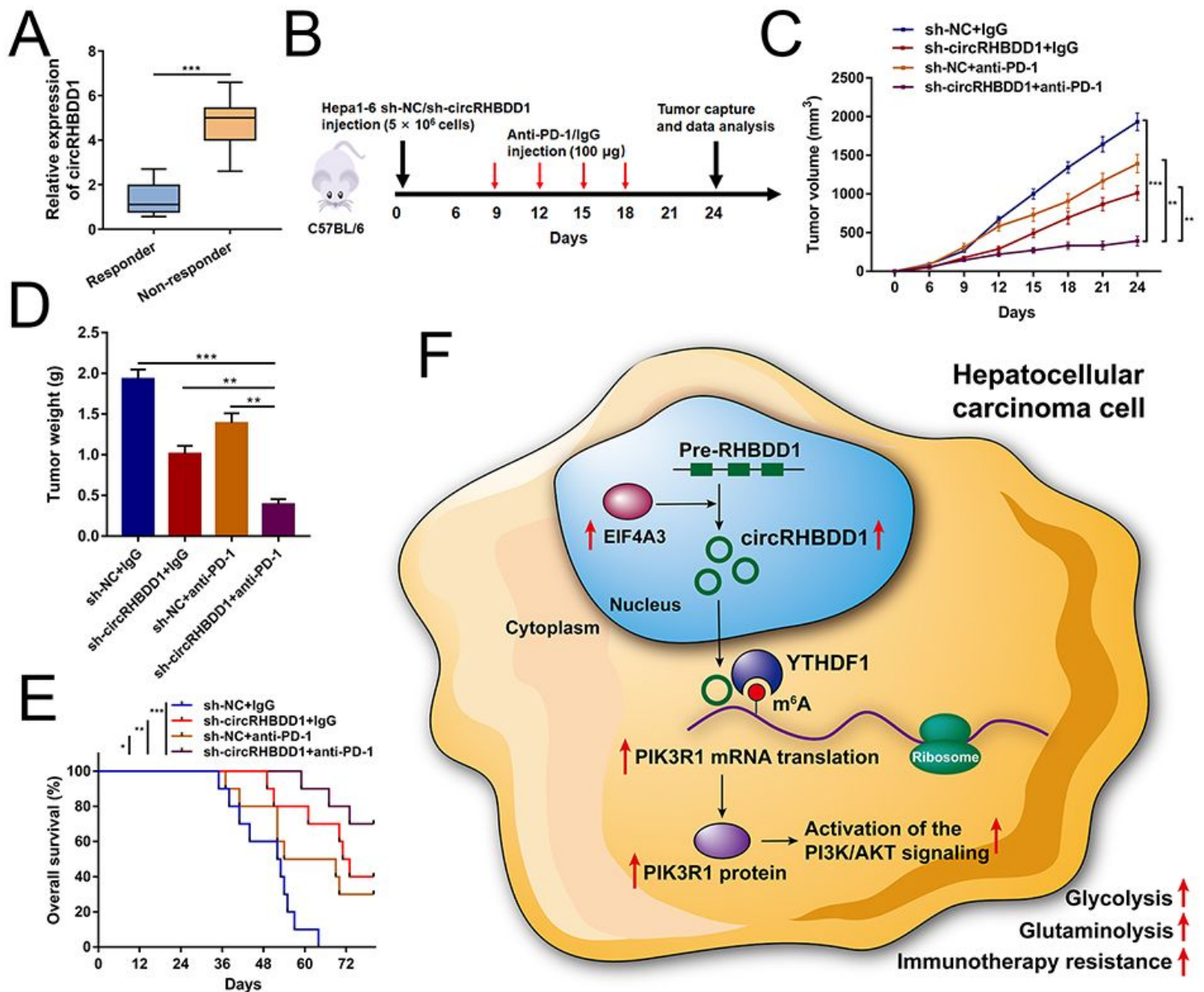

Figure 9

CircRHBDD1 restricts anti-PD-1 therapy in HCC. a The expression level of circRHBDD1 in the responder group and the non-responder group (n = 18). b Illustration of the treatment plan for CB57L/6 mice subcutaneously transplanted with circRHBDD1-silenced or control Hepa1-6 cells. c Tumor volume was measured in the engrafted tumors. d Tumor weight was recorded in the engrafted tumors. e Survival curves of mice transplanted with circRHBDD1 knockdown or control Hepa1-6 cells and treated with anti-PD1 or IgG. f A schematic diagram of this study is shown. CircRHBDD1 recruits YTHDF1 to PIK3R1 mRNA and augments PIK3R1 translation in an m6A-dependent manner, thereby promoting metabolic reprogramming and restricting anti-PD-1 therapy in hepatocellular carcinoma. EIF4A3-mediated exon back-splicing contributed to the upregulation of circRHBDD1. * P < 0.05; ** P < 0.01; *** P < 0.001.

Supplementary Files

This is a list of supplementary files associated with this preprint. Click to download.

- Additionalfile1TableS1.docx
- Additionalfile2Supplementarymethods.docx
- Additionalfile3TableS2.docx
- Additionalfile4TableS3.docx
- Additionalfile5FigureS1.tif
- Additionalfile6FigureS2.tif
- Additionalfile7FigureS3.tif
- Additionalfile8FigureS4.tif
- Additionalfile9FigureS5.tif
- Additionalfile10FigureS6.tif
- Additionalfile11FigureS7.tif
- Additionalfile12FigureS8.tif
- Additionalfile13FigureS9.tif